OPEN

Oncogene (2016) **35,** 5977–5988

www.nature.com/onc

ORIGINAL ARTICLE

Phosphorylation of serine 367 of FOXC2 by p38 regulates ZEB1 and breast cancer metastasis, without impacting primary tumor growth

SJ Werden[1,10], N Sphyris[1,10], TR Sarkar[1], AN Paranjape[1], AM LaBaff[2], JH Taube[1,11], BG Hollier[1,12], EQ Ramirez-Peña[1], R Soundararajan[1], P den Hollander[1], E Powell[3], GV Echeverria[3], N Miura[4], JT Chang[5], H Piwnica-Worms[3], JM Rosen[6,7] and SA Mani[1,8,9]

Metastatic competence is contingent upon the aberrant activation of a latent embryonic program, known as the epithelial–mesenchymal transition (EMT), which bestows stem cell properties as well as migratory and invasive capabilities upon differentiated tumor cells. We recently identified the transcription factor FOXC2 as a downstream effector of multiple EMT programs, independent of the EMT-inducing stimulus, and as a key player linking EMT, stem cell traits and metastatic competence in breast cancer. As such, FOXC2 could serve as a potential therapeutic target to attenuate metastasis. However, as FOXC2 is a transcription factor, it is difficult to target by conventional means such as small-molecule inhibitors. Herein, we identify the serine/threonine-specific kinase p38 as a druggable upstream regulator of FOXC2 stability and function that elicits phosphorylation of FOXC2 at serine 367 (S367). Using an orthotopic syngeneic mouse tumor model, we make the striking observation that inhibition of p38-FOXC2 signaling selectively attenuates metastasis without impacting primary tumor growth. In this model, circulating tumor cell numbers are significantly reduced in mice treated with the p38 inhibitor SB203580, relative to vehicle-treated counterparts. Accordingly, genetic or pharmacological inhibition of p38 decreases FOXC2 protein levels, reverts the EMT phenotype and compromises stem cell attributes *in vitro*. We also identify the EMT-regulator ZEB1—known to directly repress *E-cadherin/CDH1*—as a downstream target of FOXC2, critically dependent on its activation by p38. Consistent with the notion that activation of the p38-FOXC2 signaling axis represents a critical juncture in the acquisition of metastatic competence, the phosphomimetic FOXC2(S367E) mutant is refractory to p38 inhibition both *in vitro* and *in vivo*, whereas the non-phosphorylatable FOXC2(S367A) mutant fails to elicit EMT and upregulate ZEB1. Collectively, our data demonstrate that FOXC2 regulates EMT, stem cell traits, ZEB1 expression and metastasis in a p38-dependent manner, and attest to the potential utility of p38 inhibitors as antimetastatic agents.

Oncogene (2016) **35,** 5977–5988; doi:10.1038/onc.2016.203; published online 13 June 2016

INTRODUCTION

More than 90% of cancer-related deaths are attributed to metastases rather than primary tumors.[1] In carcinomas, metastatic competence is contingent upon the aberrant activation of a latent embryonic program, termed the epithelial–mesenchymal transition (EMT).[2] EMT is a complex process entailing reprogramming of differentiated epithelial cells toward a mesenchymal phenotype underscored by the loss of E-cadherin, reorganization of the actin cytoskeleton, acquisition of mesenchymal markers and enhanced migratory and invasive potential. Moreover, the induction of EMT in tumor cells confers self-renewal capabilities.[3,4] Cumulatively, these properties lead to *de novo* generation of metastasis-competent cancer stem cells (CSCs) that can navigate/complete the metastatic cascade and seed new tumor colonies at distal sites.

We recently identified the Forkhead transcription factor FOXC2 as a key downstream effector of multiple EMT programs, independent of the nature of the EMT-inducing stimulus.[5,6] In addition, we found that FOXC2 is necessary and sufficient for the acquisition of CSC properties, chemotherapy resistance and metastatic competence following EMT induction.[5,6] Importantly, FOXC2 expression is elevated in metastasis-prone basal-like and claudin-low CSC-enriched breast cancers,[6] as well as in residual tumor cells isolated from breast cancer patients treated with conventional therapies, which display mesenchymal and stem cell features.[7] Collectively, these findings underscore the clinical relevance of FOXC2 as a potential therapeutic target for metastatic and therapy-resistant breast cancers. However, translating these findings into an effective therapeutic modality is problematic as FOXC2 is a transcription factor, which—from a pharmacological

[1]Department of Translational Molecular Pathology, The University of Texas MD Anderson Cancer Center, Houston, TX, USA; [2]Molecular and Cellular Oncology, The University of Texas MD Anderson Cancer Center, Houston, TX, USA; [3]Department of Cancer Biology, The University of Texas MD Anderson Cancer Center, Houston, TX, USA; [4]Department of Biochemistry, Hamamatsu University School of Medicine, Hamamatsu, Japan; [5]Department of Integrative Biology and Pharmacology, University of Texas Health Science Center at Houston, Houston, TX, USA; [6]Program in Developmental Biology, Baylor College of Medicine, Houston, TX, USA; [7]Department of Molecular and Cellular Biology, Baylor College of Medicine, Houston, TX, USA; [8]Metastasis Research Center, The University of Texas MD Anderson Cancer Center, Houston, TX, USA and [9]Center for Stem Cell and Developmental Biology, The University of Texas MD Anderson Cancer Center, Houston, TX, USA. Correspondence: Dr SA Mani, Department of Translational Molecular Pathology, The University of Texas MD Anderson Cancer Center, 2130 W Holcombe Boulevard, Houston, TX 77030, USA.
E-mail: smani@mdanderson.org
[10]These authors share co-first authorship of this work.
[11]Present address: Baylor University, Waco, TX 76798, USA.
[12]Present address: Australian Prostate Cancer Research Centre-Queensland, Queensland University of Technology, Brisbane, Queensland 4102, Australia.
Received 11 September 2015; revised 31 March 2016; accepted 22 April 2016; published online 13 June 2016

standpoint—hinders rational drug design. Therefore, the identification of druggable upstream regulators of FOXC2 function may hold the key to developing effective therapies against metastatic breast cancers. However, a druggable upstream kinase that mediates FOXC2 phosphorylation, and governs its pleiotropic roles during metastatic progression, has yet to be identified.

In this work, we identify the serine/threonine-specific protein kinase p38alpha (also known as mitogen-activated protein kinase 14 (MAPK14), hereafter p38) as a critical regulator of FOXC2 stability and function, in the context of cells with mesenchymal and stem cell traits. Mechanistically, our results link p38–FOXC2 crosstalk to the activation of multiple independent EMT programs underpinning the acquisition of stem cell properties and metastatic competence. We also identify the EMT-activator ZEB1 as a downstream target of FOXC2, critically dependent on p38-mediated phosphorylation of FOXC2 at serine 367 (S367). Strikingly, whereas inhibition of p38 has little to no effect on primary tumor growth, it significantly impedes metastasis. Taken together, our findings contribute valuable insight into the poorly understood regulation of FOXC2-dependent metastasis, and unveil a selective therapeutic vulnerability of metastases to p38 inhibitors compared with primary tumors.

RESULTS

FOXC2 expression correlates with p38 activation in cells displaying mesenchymal and stem cell traits

To identify kinases that might regulate FOXC2 function, we analyzed its amino acid sequence for putative phosphorylation sites using Scansite, an online search engine that identifies short protein sequence motifs likely to be phosphorylated by known serine/threonine and tyrosine kinases.[8] Under high stringency conditions, we identified an evolutionarily well-conserved consensus phosphorylation motif for p38 associated with the S367 residue of FOXC2 (Figure 1a).

As FOXC2 expression is restricted to cells with stem cell properties,[6] we reasoned that, if p38 were a major upstream positive regulator of FOXC2 function, the active/phosphorylated form of p38, phospho-p38 (p-p38), would positively correlate with the protein levels of FOXC2. Therefore, we analyzed immortalized human mammary epithelial (HMLE) cells,[9] experimentally induced to undergo EMT via ectopic expression of Snail, Twist, transforming growth factor-β1 (TGFβ1) or Goosecoid (GSC) and two CSC-enriched human breast cancer cell lines (SUM159, MDA-MB-231), known to express high levels of endogenous FOXC2.[3,6] Using immunoblotting (Figure 1b) and immunofluorescence (Supplementary Figure S1a), we detected significantly elevated levels of p-p38 in FOXC2-expressing stem cell-enriched mesenchymal mammary cell lines relative to their more differentiated, epithelial counterparts (HMLE-vector, MCF7) (Figure 1b; Supplementary Figure S1a). Of note, we found comparable total levels of p38 in all cases (Figure 1b).

To examine the functional relationship between p-p38 and FOXC2, we treated a series of cell lines with the pyridinylimidazole SB203580 that inhibits p38 catalytic activity by binding to the ATP-binding pocket, without preventing p38 phosphorylation by upstream kinases.[10] Relative to vehicle-treated controls, SB203580 elicited a consistent and striking decrease in FOXC2 protein levels, suggesting that p38 regulates FOXC2 steady-state levels (Figure 1c; Supplementary Figure S1b). To confirm the involvement of p38, we used shRNA that decreased p38 levels by 50–70% and observed a significant reduction in FOXC2 protein levels compared with control shRNA (Figure 1d). Importantly, neither SB203580 nor p38 shRNA had a discernible effect on *FOXC2* RNA transcript levels (Supplementary Figures S1c and d). In addition, the proteasome inhibitor MG132 rescued the proteolytic degradation of FOXC2 following SB203580 treatment (Figure 1e).

Consistent with the activation of EMT at sites of wounding,[11,12] we found that p-p38 and FOXC2 accumulated in the nuclei of cells at the leading edge of a scratch induced in an epithelial HMLE cell monolayer, 9 h post wound induction (Figure 1f). Moreover, SB203580 treatment abrogated the upregulation of FOXC2 at the leading edge (but not of p-p38 as SB203580 does not impact p38 phosphorylation). Collectively, these findings reveal a striking correlation between the presence of p-p38 and FOXC2 expression in cells displaying mesenchymal and stem cell traits, as well as in mammary epithelial cells induced to undergo EMT during wound-healing, and suggest that p38 regulates FOXC2 protein levels through a post-translational mechanism.

Targeting p38 selectively inhibits metastasis leaving primary tumor growth unabated

Given the role of FOXC2 in bestowing metastatic competence,[5,6] the above data suggest that disrupting the p38–FOXC2 interaction, using a p38-inhibitor, may perturb tumor progression. In order to investigate this, we employed the 4T1 mouse mammary carcinoma model, which recapitulates many of the characteristics of human breast cancer. Most notably, 4T1 cells can spontaneously metastasize from a site of orthotopic implantation—the mammary gland—to the lung in syngeneic wild-type immunocompetent mouse hosts.[13,14]

First, we confirmed a significant reduction of endogenous FOXC2 protein levels following treatment of 4T1 cells with SB203580 (Figure 2a). Next, we orthotopically implanted red-fluorescent-protein-(RFP)/luciferase-labeled 4T1 cells into the fourth mammary fat pads of 40 female BALB/c mice and subsequently administered vehicle or SB203580 subcutaneously (20 mice per group). We monitored tumor progression weekly using caliper measurements and bioluminescence. Starting week 3 post-implantation, we killed five mice per group and surgically excised the primary tumors and lungs. Unexpectedly, SB203580-treated mice formed primary tumors of a similar size relative to vehicle-treated counterparts (Figure 2b, left panels). This observation was corroborated by caliper measurements (Figure 2c) and the bioluminescent signal emitted by these tumors (Supplementary Figures S2a and b). Contrary to our observations with primary tumors, mice treated systemically with SB203580 exhibited strikingly fewer lung metastases, as evidenced by the markedly reduced bioluminescent signal relative to vehicle-treated counterparts (Figure 2b, right panels, and Figure 2d). Consistent with these observations, macroscopic and histological examination revealed the presence of multiple nodules in the lungs of vehicle-treated mice compared with much fewer nodules in the lungs of SB203580-treated counterparts (Supplementary Figures S2c and d). Collectively, these findings suggest that p38 inhibition selectively prevents metastasis, without impacting primary tumor formation and growth.

We also collected blood from vehicle- and SB203580-treated counterparts, during the 3–6-week post-implantation period, and quantified the number of viable circulating tumor cells (CTCs) isolated from the blood and cultured as RFP-positive colonies. Strikingly, while we were able to recover CTCs from vehicle-treated mice, even 3 weeks post-implantation, we were unable to detect any CTCs in the blood of SB203580-treated mice until week 5, and in week 6, we recovered only very few CTCs from SB203580-treated mice (Figure 2e).

Interestingly, both p38 and FOXC2 have been implicated in tumor angiogenesis.[15,16] However, our analyses of microvessel density—quantified by CD31 immunohistochemistry and image analysis—did not reveal significant differences in the vasculature of primary tumors from SB203580-treated mice compared with vehicle-treated counterparts (data not shown), which might have explained the lack of CTCs in SB203580-treated mice. These

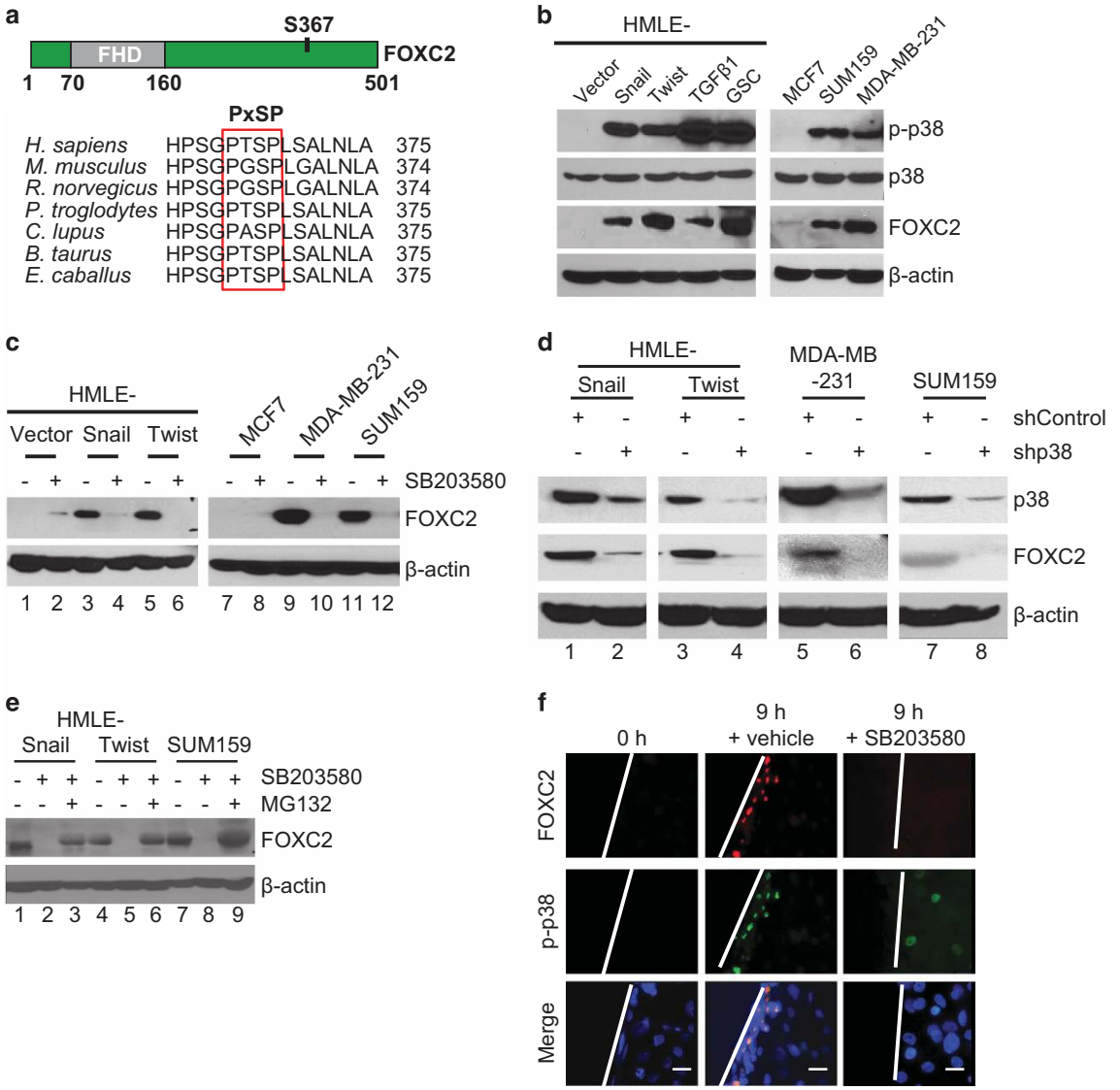

Figure 1. FOXC2 expression correlates with p38 activation in cells with mesenchymal and stem cell properties. (**a**) Alignment of FOXC2 amino acid sequences from multiple species shows high evolutionary sequence conservation at S367, the putative phosphorylation site for p38. (**b**) Cell lysates from the indicated cells were analyzed by immunoblotting for p-p38, p38 and FOXC2. β-Actin was used as a loading control. (**c**) The indicated cells were treated with vehicle or SB203580 for 24 h. Cell lysates were analyzed by immunoblotting for FOXC2. β-Actin was used as a loading control. (**d**) The indicated cells were transduced with p38 shRNA (shp38) or control shRNA (shControl). Cell lysates were analyzed by immunoblotting for p38 and FOXC2. β-Actin was used as a loading control. (**e**) Pretreatment of the indicated cells with 10 μM MG132 prevents the proteolytic degradation of FOXC2 following SB203580 treatment, as determined by immunoblotting. β-Actin was used as a loading control. (**f**) For the scratch/wound-healing assay, a confluent monolayer culture of epithelial HMLE cells was scratched with a sterile pipette tip. HMLE cells were treated with vehicle or SB203580 and fixed immediately following scratch induction (0 h) or 9 h post wound induction, followed by immunostaining for FOXC2 (red) and p-p38 (green). Nuclei were counterstained with 4,6-diamidino-2-phenylindole (DAPI; blue). Scale bar, 20 μm.

findings suggest that p38 inhibition compromises the intravasation of CTCs or the survival of CTCs in the circulation.

As many breast cancer patients harbor occult micrometastases, at the time of diagnosis, and metastasis is often attributed to the systemic dissemination of tumor cells before or during surgical resection of the primary tumor,[17,18] we examined whether p38 inhibition could also prevent colonization and progression to macrometastasis. For this, we employed an experimental metastasis model, which circumvents the early steps of the metastatic cascade. We injected luciferase-labeled MDA-MB-231 cells, via the tail vein of NOD/SCID mice, and monitored the emergence of lung metastases using bioluminescence. In concordance with our observations using the 4T1 model, injection of SB203580 daily, beginning 48 h post-injection, significantly reduced the metastatic burden and extended event-free survival compared with vehicle-treated mice (Supplementary Figures S3a and b). To eliminate the possibility of 'off-target' effects, we intravenously injected mice with MDA-MB-231 cells expressing either control shRNA or p38 shRNA. Similar to our findings with SB203580, shRNA-mediated suppression of p38 drastically impaired lung colonization, relative to control shRNA-expressing counterparts, and significantly prolonged event-free survival (Supplementary Figures S3c and d). These data suggest that p38 inhibition could also curtail colonization at the distant site. We conclude that, whereas p38

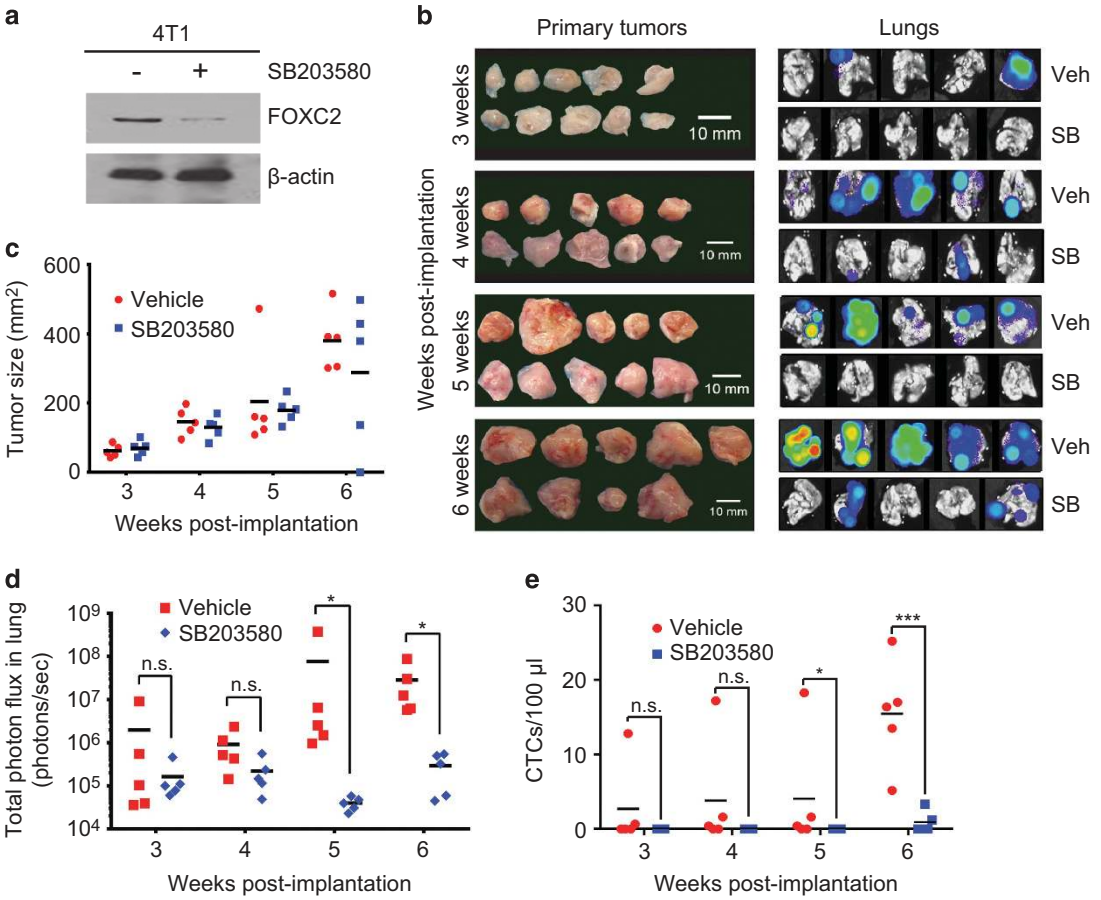

Figure 2. p38 inhibition leaves primary tumor growth unabated but significantly compromises metastasis. (**a**) 4T1 cells were treated with vehicle or SB203580 for 24 h. Cell lysates were analyzed by immunoblotting for FOXC2, with β-actin as a loading control. (**b**) Luciferase-labeled 4T1 cells were orthotopically injected into mice, subsequently treated daily with vehicle or SB203580. Primary mammary tumors (left panel; macroscopic) and lungs (right panel; bioluminescence) were harvested at 3, 4, 5 and 6 weeks post-implantation. $n = 5$ mice per group. (**c**) The size of the primary mammary tumors, harvested from mice in panel (**b**), was measured with a caliper as the product of two perpendicular diameters (mm^2) and plotted over time. (**d**) The bioluminescent signal from the lungs in panel (**b**) was quantified to determine the incidence of metastases. (**e**) The number of CTCs per 100 µl of blood, isolated from mice in panel (**b**), and cultured as RFP-positive colonies *in vitro* was quantified and plotted over time. *P*-values were calculated using Student's unpaired two-tailed *t*-test. $^*P \leqslant 0.05$; $^{***}P < 0.001$ compared with the control. n.s., not significant.

Figure 3. p38 inhibition compromises the acquisition and maintenance of EMT and stem cell properties *in vitro*. (**a**) MCF10A cells were treated with TGFβ1 alone, or in combination with SB203580, for 3 days. The cells were harvested, and the corresponding lysates were analyzed by immunoblotting for FOXC2, E-cadherin and mesenchymal markers. β-Actin was used as a loading control. (**b**) HMLE-Snail-ER cells were treated with 4-OHT for 12 days and concurrently exposed to vehicle or SB203580. Cells were harvested at the indicated time points and the corresponding lysates were analyzed by immunoblotting for FOXC2, E-cadherin and mesenchymal markers. β-Actin was used as a loading control. (**c**) HMLE-Snail-ER and HMLE-Twist-ER cells were treated with 4-OHT for 12 days and concurrently exposed to vehicle or SB203580. One thousand cells were seeded per well in ultra-low attachment plates and cultured for 7–10 days. Spheres with a diameter >75 µm were counted. The data are reported as the number of spheres formed/1000 seeded cells ± s.e.m. (**d**) The percentage of $CD44^{high}/CD24^{low}$ cells in 4-OHT-treated HMLE-Snail-ER and HMLE-Twist-ER populations, concurrently exposed to vehicle or SB203580, was determined by fluorescence-activated cell sorting (FACS). Data are presented as mean ± s.e.m. (**e**) HMLE-Twist-ER cells, transduced with *p38* shRNA (shp38) or control shRNA (shControl), were treated with 4-OHT for 9 days and harvested at the indicated time points. The corresponding lysates were analyzed by immunoblotting for FOXC2, E-cadherin and mesenchymal markers. β-Actin was used as a loading control. (**f**) The sphere-forming efficiency of 4-OHT-treated HMLE-Twist-ER cells, transduced with control shRNA (shControl) or p38 shRNA (shp38), was determined. The data are reported as the number of spheres formed/1000 seeded cells ± s.e.m. (**g**) The indicated cells were treated with vehicle or SB203580, and the corresponding lysates were analyzed by immunoblotting for FOXC2, E-cadherin and mesenchymal markers. β-Actin was used as a loading control. (**h**) The sphere-forming efficiency of the indicated cells was determined in the presence of vehicle or SB203580. The data are reported as the number of spheres formed/1000 seeded cells ± s.e.m. (**i**) The percentage of $CD44^{high}/CD24^{low}$ subpopulations in the indicated cells, treated with vehicle or SB203580, was determined by FACS. Data are presented as mean ± s.e.m. (**j**) The relative wound closure by the indicated cells, treated with vehicle or SB203580, was measured by image analysis and represented in a graphical format. Data are presented as mean ± s.e.m. (**k**) The relative wound closure by HMLE cells, transduced with control shRNA (shControl), p38 shRNA (shp38) or FOXC2 shRNA (shFOXC2), was measured by image analysis and represented in a graphical format. Data are presented as mean ± s.e.m. (**l**) HMLE-Snail and HMLE-Twist cells were plated on fluorescein isothiocyanate (FITC)-conjugated gelatin and treated with vehicle or SB203580. After 16 h, the cells were fixed and stained with fluorescent phalloidin, and the nuclei were counterstained with DAPI to facilitate visualization of the cells (see Supplementary Figure S4b). Degradation of FITC–gelatin was quantified by image analysis. $n = 150$ cells/sample. Data are reported as mean ± s.e.m. *P*-values were calculated using Student's unpaired two-tailed *t*-test. $^*P < 0.05$; $^{**}P < 0.01$; $^{***}P < 0.001$ compared with the control.

inhibition does not significantly affect primary tumor growth, it negatively impacts CTC numbers, lung colonization and, ultimately, metastasis.

p38 inhibition compromises EMT and stem cell traits *in vitro*

The above findings suggested that p38 might regulate specific cellular attributes associated with the ability to navigate/complete the invasion-metastasis cascade.[19] As FOXC2 knockdown prevents EMT and the acquisition of stem cell properties,[6] we investigated the impact of p38 inhibition on these intertwined processes.

To ascertain whether inhibiting p38 impedes the initiation of EMT, we utilized two dynamic models of EMT induction. First, we treated MCF10A immortalized human mammary epithelial cells with TGFβ1, which elicits EMT. We found that inhibition of p38, by concomitant SB203580 treatment, suppresses the upregulation of FOXC2 and mesenchymal markers (fibronectin, vimentin) and prevents downregulation of the epithelial marker E-cadherin in TGFβ1-treated cells (Figure 3a). Second, we used an inducible EMT system wherein a fusion protein, comprising the EMT-inducing transcription factors Snail or Twist and the estrogen-binding domain of the estrogen receptor (ER), is stably expressed in epithelial HMLE cells (HMLE-Snail-ER, HMLE-Twist-ER). Addition of the ER-ligand 4-hydroxy-tamoxifen (4-OHT) promotes nuclear translocation of the Snail-ER and Twist-ER proteins and elicits

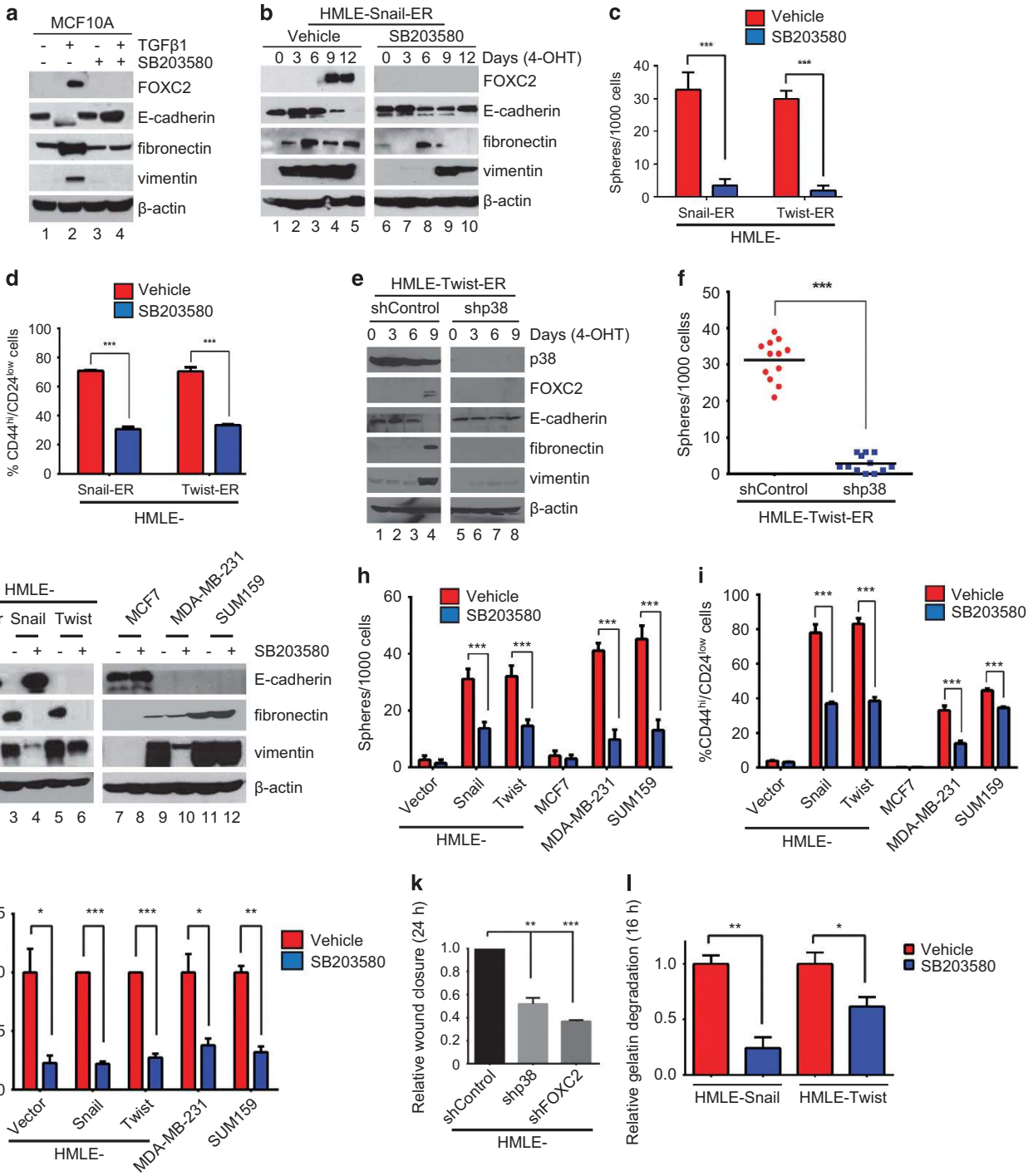

EMT.[3] Although 4-OHT treatment alone instigated EMT (Figure 3b, lanes 4 and 5), HMLE-Snail-ER cells, concurrently exposed to 4-OHT and SB203580, failed to undergo EMT or upregulate FOXC2 (Figure 3b, lanes 9 and 10). Additionally, following SB203580 exposure, 4-OHT-treated HMLE-Snail-ER and HMLE-Twist-ER cells failed to acquire sphere-forming potential (Figure 3c) and the $CD44^{high}/CD24^{low}$ marker profile (Figure 3d), functional and phenotypic indicators of stemness respectively. Similarly, p38 shRNA abolished the capacity of HMLE-Twist-ER cells to undergo EMT (Figure 3e, compare lane 4 with lane 8) and to form spheres (Figure 3f) in response to 4-OHT treatment. Collectively, these results suggest that p38 inhibition compromises the initiation of EMT and the acquisition of stem cell attributes elicited by well-known EMT-inducers.

We next ascertained whether p38 inhibition compromises the maintenance of the established EMT phenotype. Indeed, we found that exposure of mesenchymal HMLE-Snail, HMLE-Twist, MDA-MB-231 and SUM159 cells to SB203580 elicited various degrees of inhibition of mesenchymal and stem cell traits (Figures 3g–l). Thus, SB203580 treatment altered the expression of EMT markers (Figure 3g, Supplementary Figure S4a), and substantially reduced sphere formation (Figure 3h) and the percentage of cells displaying the $CD44^{high}/CD24^{low}$ antigenic profile (Figure 3i), relative to vehicle-treated cells.

Consistent with the fact that EMT confers increased migratory potential, SB203580 markedly reduced the migratory capacity of mesenchymal cells in a scratch/wound-healing assay (Figure 3j). Moreover, HMLE cells, expressing shRNAs targeting p38 or FOXC2, displayed markedly reduced migratory capacity compared with control shRNA counterparts (Figure 3k). These results argue for an important role of p38-mediated phosphorylation of FOXC2 in eliciting wound closure, consistent with our earlier observations that FOXC2 nuclear staining is lacking at the leading edge of wounded SB203580-treated HMLE monolayers (Figure 1f) that failed to repopulate the void created by the scratch (data not shown). We also investigated the effects of p38 inhibition on invasive potential, which strongly correlates with the formation of invadopodia.[20] These specialized actin-based cell membrane protrusions secrete matrix metalloproteinases, enabling degradation of the nearby extracellular matrix.[20] We quantified the formation of invadopodia by assessing the ability of cells to degrade fluorescein isothiocyanate-conjugated gelatin.[20] Using this assay, we found that vehicle-treated HMLE-Snail and HMLE-Twist cells degraded the underlying extracellular matrix within 16 h, whereas SB203580-treated counterparts failed to do so to the same degree (Figure 3l; Supplementary Figure S4b). Collectively, these results suggest that p38 signaling not only has a critical role in the initiation of the EMT programs instigated by various EMT-inducers, but also that it actively sustains the maintenance of EMT and the stem cell attributes it confers.

p38 phosphorylates FOXC2 at S367

To determine whether p38 and FOXC2 interact with one another, we co-expressed HA-tagged p38 and Myc-tagged FOXC2 in HEK293T cells, immunoprecipitated for either HA or Myc, and analyzed the resulting immunoprecipitates by immunoblotting with Myc and HA antibodies respectively (Supplementary Figures S5a and b). These data confirmed the interaction between FOXC2 and p38, which is contingent on the activation status of p38, as it was abolished when a kinase-dead mutant of p38 (HA-p38-DN) was substituted during transfection (Supplementary Figure S5b). This suggests that, among other factors, the interaction of p38 with FOXC2 depends on the configuration of the p38 catalytic cleft. To confirm that FOXC2 serves as a p38 substrate, we performed an *in vitro* kinase assay (Figure 4a). Indeed, p38-dependent phosphorylation of FOXC2 was detected with N-terminally truncated FOXC2, comprising amino acids 245–501, but not with a C-terminally truncated FOXC2, numbering amino acids 1–244, devoid of the putative p38 phosphorylation site. Moreover, FOXC2 phosphorylation was not observed when S367 was mutated to a non-phosphorylatable alanine residue (Figure 4a). Collectively, these data suggest that p-p38 physically interacts with FOXC2 and phosphorylates FOXC2 at S367.

p38 controls EMT and stem cell traits via FOXC2

Having established that FOXC2 is a p38 substrate, we sought to determine whether phosphorylation of FOXC2 on S367 is critical for the acquisition of EMT and stem cell traits. For this, we generated phosphomimetic FOXC2(S367E) and non-phosphorylatable FOXC2(S367A) mutants and evaluated their ability to bestow mesenchymal and stem cell traits relative to wild-type FOXC2 (referred to as FOXC2). Both FOXC2 and FOXC2(S367E) elicited EMT in Ras-transformed HMLE cells (HMLER), as evidenced by the acquisition of an elongated, spindle-shaped morphology (Figure 4b), loss of E-cadherin and gain of mesenchymal markers (Figure 4c, lanes 2 and 3). Conversely, the FOXC2(S367A) mutant—even though it was expressed at comparable levels—failed to induce EMT (Figures 4b and c, lane 4). Furthermore, ectopic expression of either FOXC2 or the FOXC2(S367E) mutant enhanced the sphere-forming potential of HMLER cells (Figure 4d) and promoted a shift toward the $CD44^{high}/CD24^{low}$ antigenic profile (Figure 4e).[21] Moreover, whereas SB203580 reduced—as anticipated—the sphere-forming capacity of HMLER-FOXC2 cells, HMLER-FOXC2(S367E) cells retained the ability to form spheres even in the presence of SB203580 (Figure 4f). In the aforementioned assays, the non-phosphorylatable FOXC2(S367A) mutant did not promote sphere formation (Figures 4d and f) and was associated with the $CD44^{low}/CD24^{high}$ epithelial cell-surface marker profile (Figure 4e). Finally, whereas SB203580 inhibited the migration of HMLER-vector ($>70\%$) and HMLER-FOXC2 ($>70\%$) cells, HMLER-FOXC2(S367E) cells exhibited only a modest decrease ($<30\%$) in wound closure (Figure 4g). Collectively, these findings demonstrate that p38-mediated phosphorylation of the S367 residue of FOXC2 empowers it to confer combined EMT and stem cell attributes *in vitro*.

p38-mediated phosphorylation of FOXC2 promotes metastasis

We next tested whether p38-mediated phosphorylation of FOXC2 enhances its ability to confer metastatic competence. First, we demonstrated that, whereas SB203580 treatment of vector-transduced 4T1 cells abolished endogenous FOXC2 protein levels, the phosphomimetic FOXC2(S367E) levels remained unaltered (Figure 5a). Accordingly, whereas SB203580 compromised the sphere-forming efficiency of vector-transduced 4T1 cells, 4T1-FOXC2(S367E) cells retain a significant level of sphere-forming ability even in the presence of SB203580 (Figure 5b).

Next, we orthotopically implanted luciferase-labeled 4T1 cells, expressing empty vector or FOXC2(S367E), into the mammary fat pads of BALB/c mice and subsequently treated these mice with SB203580. Similar to our earlier findings, there were no significant differences in primary tumor growth following SB203580 treatment in mice harboring 4T1-vector or 4T1-FOXC2(S367E) cells (Figure 5c). Moreover, the incidence of lung metastases in SB203580-treated mice, harboring 4T1-vector cells, was reduced by >20-fold compared with vehicle-treated counterparts (Figures 5d and e). In sharp contrast, numerous lung nodules could be detected in mice harboring 4T1-FOXC2(S367E) cells, and most importantly, SB203580 failed to significantly reduce the metastatic burden (Figures 5d and e), compared with the vehicle-treated 4T1-vector and 4T1-FOXC2(S367E) counterparts.

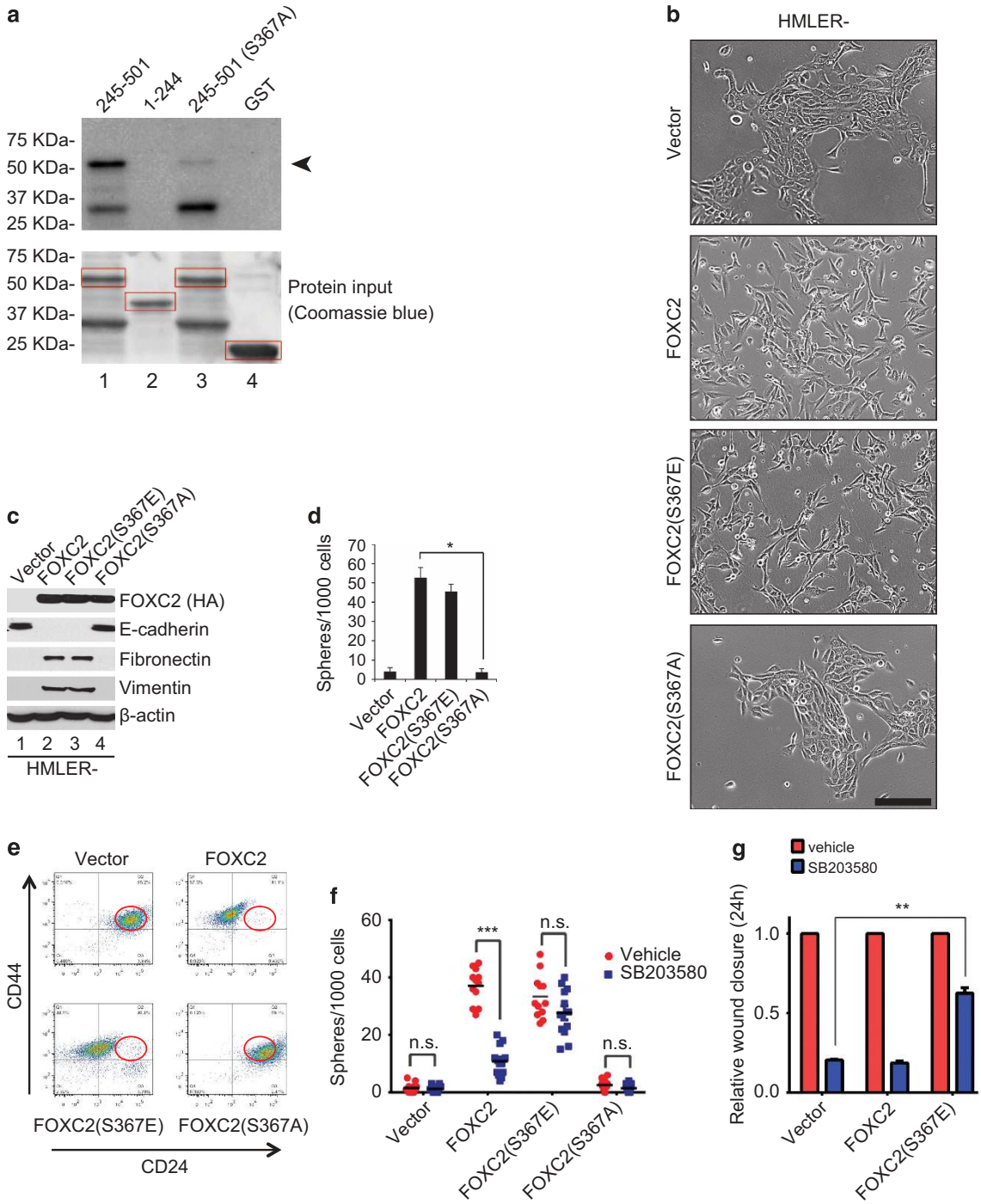

Figure 4. EMT and stem cell properties of HMLER cells expressing FOXC2(S367) mutants. (**a**) Recombinant GST-FOXC2 fusion proteins: N-terminally truncated FOXC2 (amino acids 245–501), C-terminally truncated FOXC2 (amino acids 1–244), or N-terminally truncated FOXC2 (amino acids 245–501) with alanine substitution at serine 367 (S367A), were purified from *E. coli* using glutathione-sepharose-4B beads. The respective eluates were subjected to *in vitro* kinase assays with recombinant active p38. The reaction mixtures were resolved by SDS–PAGE, and the phosphorylated proteins were visualized by autoradiography. The electrophoretic mobility of phosphorylated GST-FOXC2 is indicated with an arrowhead. The GST control and the C-terminally truncated FOXC2 (amino acids 1–244), devoid of the putative p38 phosphorylation site, did not show any phosphorylation in this assay. The bottom panel depicts Coomassie blue staining of the protein input. (**b**) HMLER cells were transduced with empty vector, FOXC2, FOXC2(S367E) or FOXC2(S367A), and their morphology was imaged through phase-contrast microscopy. Scale bar, 100 μm. (**c**) Cell lysates from HMLER cells, transduced with the indicated constructs, were analyzed by immunoblotting for FOXC2 (anti-HA), E-cadherin, fibronectin and vimentin. β-Actin was used as a loading control. (**d**) Sphere formation by HMLER cells, transduced with the indicated constructs, is represented as the mean number of spheres formed/1000 seeded cells ± s.e.m. (**e**) The indicated HMLER cells were analyzed by fluorescence-activated cell sorting for the presence of CD44 and CD24 on the cell surface. The circles denote the position of the vector-transduced control population in the cytograms. (**f**) Sphere formation by the indicated HMLER cells, treated with vehicle or SB203580, is represented as the mean number of spheres formed/1000 seeded cells ± s.e.m. (**g**) The relative wound closure by the indicated HMLER cells, treated with vehicle or SB203580, was measured by image analysis and represented in a graphical format. Data are presented as mean ± s.e.m. *P*-values were calculated using Student's unpaired two-tailed *t*-test. $^{*}P < 0.05$; $^{**}P < 0.01$; $^{***}P < 0.001$ compared with the control. n.s., not significant.

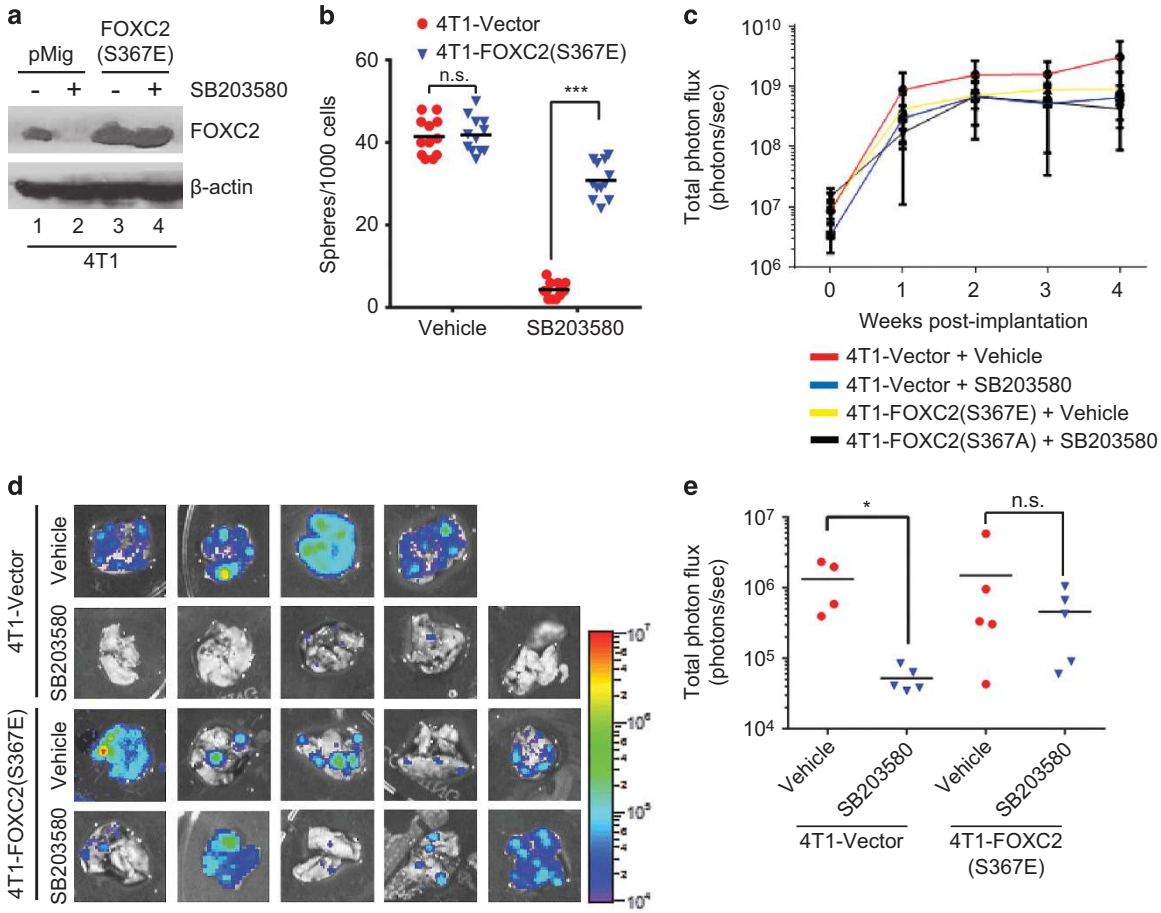

Figure 5. p38-mediated phosphorylation of FOXC2 at S367 regulates metastasis. (**a**) 4T1 cells, transduced with either empty vector (pMIG) or FOXC2(S367E), were treated with vehicle or SB203580. Cell lysates were analyzed by immunoblotting for FOXC2 (using the rat anti-mouse FOXC2 antibody that also crossreacts with human FOXC2), with β-actin as a loading control. (**b**) 4T1 cells, transduced with empty vector or FOXC2(S367E), were subjected to a sphere-formation assay in the presence of vehicle or SB203580. Data are presented as the mean number of spheres formed/1000 seeded cells ± s.e.m. (**c**) 4T1-vector or 4T1-FOXC2(S367E) luciferase-labeled cells were orthotopically injected into mice. Mice were treated daily with vehicle or SB203580, and primary tumor growth was monitored weekly by bioluminescence. Data are presented as the total photon flux plotted over time and reported as the mean ± s.e.m. (**d**) Representative bioluminescent images of lungs harvested from mice in panel (**c**) at 4 weeks post-implantation. (**e**) The bioluminescent signal from the lungs harvested from mice in panel (**c**) was quantified to determine the incidence of metastasis. Data are reported as mean ± s.e.m. *P*-values were calculated using Student's unpaired two-tailed *t*-test.*$P < 0.05$; ***$P < 0.001$ compared with the control. n.s., not significant.

Figure 6. p38-mediated phosphorylation of FOXC2 directly regulates ZEB1 expression. (**a**) The transcript levels of *FOXC2* and *ZEB1* in HMLER-vector and HMLER-FOXC2 cells were determined by qRT–PCR, with glyceraldehyde 3-phosphate dehydrogenase (*GAPDH*) as the reference gene to normalize the variability in template loading. Data are reported as mean ± s.e.m. (**b**) Cell lysates from the indicated cells were analyzed by immunoblotting for FOXC2 and ZEB1. β-Actin was used as a loading control. (**c**) HMLE-Snail and HMLE-Twist cells were immunostained with antibodies against FOXC2 (green) and ZEB1 (red). Nuclei were counterstained with DAPI (blue). Scale bar, 20 μm. (**d**) HMLE-Snail cells, transduced with control shRNA (shControl) or *FOXC2* shRNA (shFOXC2), were immunostained with antibodies against FOXC2 (green) and ZEB1 (red). Nuclei were counterstained with DAPI (blue). Scale bar, 20 μm. (**e**) The relative expression of *ZEB1* mRNA in the indicated cells, transduced with control shRNA (shControl) or *FOXC2* shRNA (shFOXC2), was determined by qRT–PCR with *GAPDH* as the reference gene. Data are reported as mean ± s.e.m. (**f**) The protein levels of FOXC2, ZEB1 and β-actin in the indicated cells, transduced with control shRNA (shControl) or *FOXC2* shRNA (shFOXC2), were analyzed by immunoblotting. (**g**) The relative levels of *miR200b* and *miR200c* in HMLER-vector and HMLER-FOXC2 cells were determined by qRT–PCR, with U6 small nuclear RNA as an internal control. Data are reported as mean ± s.e.m. (**h**) The mRNA abundance of *miR200b* and *miR200c* in HMLE-Snail cells, transduced with control shRNA (shControl) or *FOXC2* shRNA (shFOXC2), was determined by qRT–PCR, with U6 small nuclear RNA as an internal control. Data are reported as mean ± s.e.m. (**i**) The relative levels of *ZEB1* transcripts in the indicated cells, treated with vehicle or SB203580, were determined by qRT–PCR, with *GAPDH* as the reference gene. Data are reported as mean ± s.e.m. (**j**) Cell lysates from the indicated cells, treated with vehicle or SB203580, were analyzed by immunoblotting for ZEB1. β-Actin was used as a loading control. (**k**) HMLER cells were transduced with empty vector, FOXC2, FOXC2(S367E) or FOXC2(S367A). These cells were treated with vehicle or SB203580, and the corresponding lysates were analyzed by immunoblotting for ZEB1. β-Actin was used as a loading control. (**l**) A chromatin immunoprecipitation assay was performed using HMLER-FOXC2, HMLER-FOXC2(S367E) and HMLER-FOXC2(S367A) cells to show that FOXC2 binds upstream to the transcriptional start site of the *ZEB1* promoter. The *y*-axis represents the percentage of bound FOXC2, and the *x*-axis denotes the distance from the *ZEB1* transcription start site in kb. n.d., not determined. *P*-values were calculated using Student's unpaired two-tailed *t*-test. *$P < 0.05$; **$P < 0.01$; ***$P < 0.001$ compared with the control.

p38-mediated phosphorylation of FOXC2 regulates *ZEB1* expression

To identify potential downstream mediators of p-p38 and FOXC2, we analyzed our previous microarray data (GEO accession: GSE44335) from HMLER-FOXC2 cells relative to HMLER-vector counterparts[6] and identified the transcription factor *ZEB1* as one of the highly upregulated genes (116-fold) in HMLER-FOXC2 cells. We first confirmed the elevated levels of *FOXC2* and *ZEB1* transcripts in HMLER-FOXC2 cells versus HMLER-vector cells by quantitative reverse transcriptase–PCR (qRT–PCR; Figure 6a).

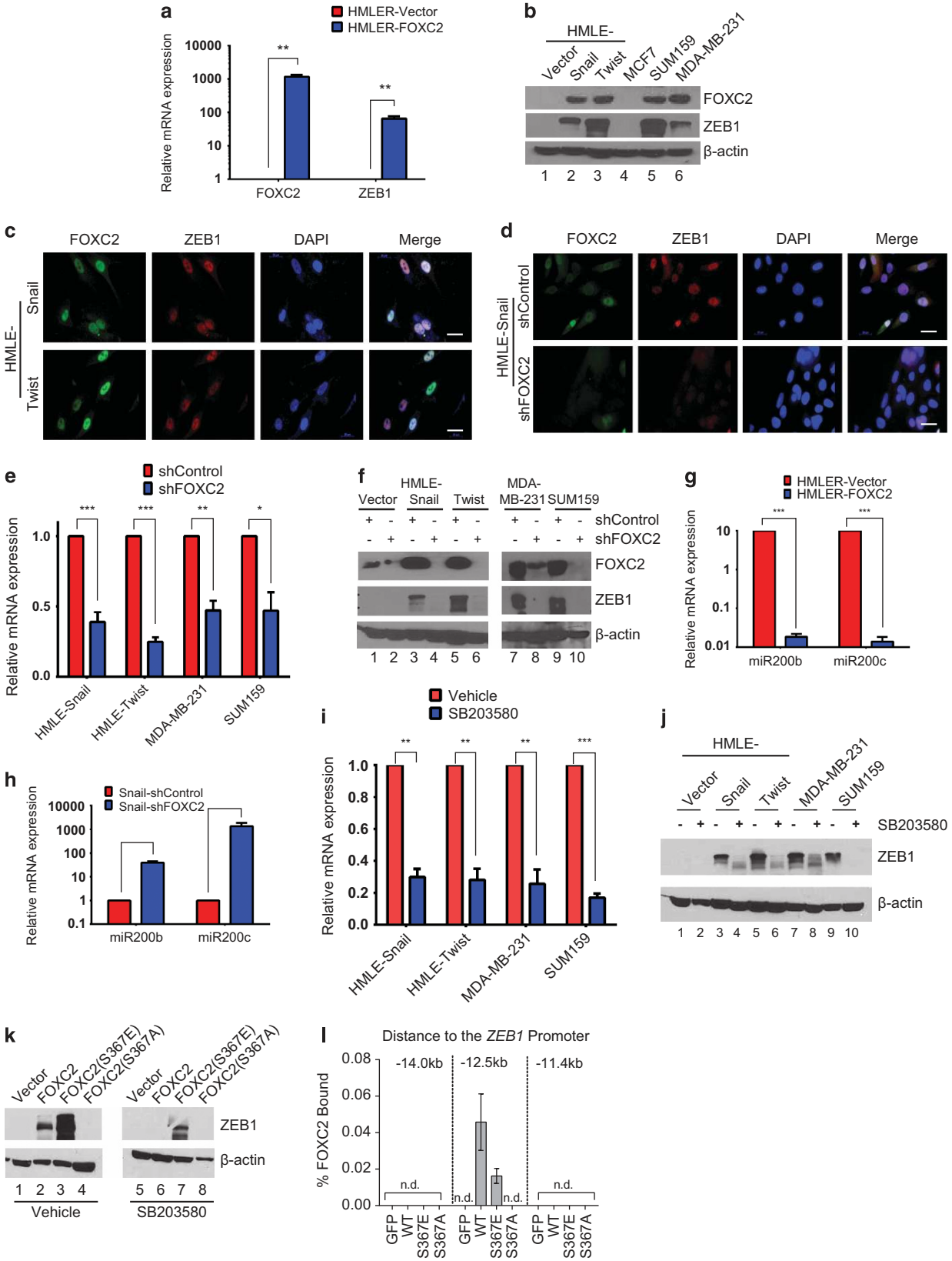

Furthermore, immunoblotting revealed a positive correlation between elevated FOXC2 and ZEB1 protein levels in cells induced to undergo EMT and CSC-enriched cell lines (Figure 6b). At the cellular level, immunofluorescence demonstrated that FOXC2 and ZEB1 co-localize in the nuclei of HMLE-Snail and HMLE-Twist cells (Figure 6c) and that *FOXC2* knockdown elicits a marked decrease in ZEB1 staining intensity (Figure 6d). Accordingly, shRNA-mediated suppression of *FOXC2* in a panel of cell lines yielded a dramatic decrease in *ZEB1* mRNA (Figure 6e) and a >80% reduction in ZEB1 protein levels (Figure 6f). Furthermore, consistent with the reciprocal regulation of *ZEB1* and miR-200 family members,[22] we observed decreased levels of *miR-200b* and *miR-200c* in HMLER-FOXC2 cells, compared with vector-transduced counterparts (Figure 6g). Conversely, we found a >50-fold increase in *miR-200b,* and a >1000-fold increase in *miR-200c*, following *FOXC2* knockdown compared with control shRNA-transduced counterparts (Figure 6h). Consistent with our findings that p38 inhibition diminishes FOXC2 expression, ZEB1 mRNA and protein levels were reduced significantly following SB203580 treatment compared with vehicle-treated cells (Figures 6i and j). Furthermore, in support of the notion that p38-mediated phosphorylation of FOXC2 regulates *ZEB1* expression, we could only detect elevated ZEB1 protein levels in HMLER-FOXC2 and HMLER-FOXC2(S367E) cells (Figure 6k, lanes 2 and 3) but not in HMLER-FOXC2(S367A) cells (Figure 6k, lane 4). Moreover, when HMLER cells expressing the FOXC2 variants were treated with SB203580, ZEB1 protein levels were decreased in HMLER-FOXC2 cells (Figure 6k, lane 6) but remained relatively high in HMLER-FOXC2(S367E) cells (Figure 6k, lane 7). To ascertain whether FOXC2 directly regulates miR-200 or *ZEB1* expression, we analyzed the promoter regions of both miR-200 clusters on chromosomes 1 and 12[23] as well as the *ZEB1* promoter and identified a conserved FOXC2-binding element within the *ZEB1* promoter. Indeed, using chromatin immunoprecipitation, we found that FOXC2 preferentially binds to a region around 12.5 kb (−12.5 kb) upstream of the *ZEB1* transcription start site (Figure 6l), thus confirming that FOXC2 is a direct transcriptional regulator of *ZEB1*. This promoter binding was also observed with the phosphomimetic FOXC2(S367E) but not the non-phosphorylatable FOXC2(S367A) (Figure 6l). To demonstrate that ZEB1 is important for the FOXC2-associated EMT/CSC properties, we silenced *ZEB1* expression using shRNA. We were thus able to demonstrate that *ZEB1* knockdown significantly diminishes mammosphere-forming ability without affecting the expression of FOXC2 and phospho-ATF2 (a downstream target of p38) (Supplementary Figure S6), indicating that ZEB1 is downstream of p38 and FOXC2. Collectively, these findings demonstrate that p38-mediated phosphorylation of FOXC2 directly regulates the expression of *ZEB1* and that ZEB1 may be an important mediator of p38-FOXC2 signaling.

DISCUSSION

We previously reported that FOXC2 is a critical regulator of EMT, stem cell properties and metastatic competence.[5,6] However, the fact that FOXC2 is a transcription factor renders it inherently difficult to inhibit pharmacologically.[24] Herein, we identify the serine/threonine-specific kinase p38 as a druggable upstream regulator of FOXC2 function. Phosphorylation of FOXC2 by p38 at S367 regulates FOXC2 protein stability, promotes expression of its downstream target ZEB1, and modulates its ability to confer EMT properties and stem cell attributes *in vitro* and metastatic competence *in vivo*.

Although p38 has been previously implicated in the regulation of multiple steps of tumor progression and the metastatic cascade,[25–27] we provide compelling evidence, using an orthotopic syngeneic mouse tumor model, that inhibition of p38-FOXC2 signaling selectively prevents metastasis without impacting primary tumor growth. These findings lend support to the notion that the growth of primary tumors and metastases is regulated by distinct signaling pathways.[28–31] Notably, in this spontaneous metastasis model, we observed that CTC numbers were significantly reduced in SB203580-treated mice, relative to vehicle-treated counterparts. Although both p38 and FOXC2 have been shown to regulate angiogenesis,[15,16] we did not observe gross differences in the vasculature of primary tumors from SB203580-treated mice and vehicle-treated counterparts, which could have accounted for the markedly reduced shedding of CTCs into the circulation. Altogether, we found that genetic or pharmacological inhibition of p38 impairs the acquisition and maintenance of the EMT phenotype, migratory potential, invadopodia formation, and stem cell attributes *in vitro* and metastases *in vivo* in mouse mammary tumor models (Figures 1–3 and 6). Similarly, inhibition of p38 in a human PDX model of triple-negative breast cancer also inhibits metastasis (data not shown). Together, these results suggest that the p38-FOXC2 signaling axis regulates metastasis at the steps leading to the *de novo* generation of metastasis-competent CSCs, destined to become CTCs upon detachment from the primary tumor.

Several studies have alluded to the existence of CSC subclasses with distinct marker profiles as well as tumor-initiating and metastatic capabilities.[32–34] Although we did not directly gauge the effects of p38-FOXC2 signaling on the representation of CSC subpopulations within the various mammary carcinoma cells studied here, our findings support the existence of two CSC-subtypes: CSCs with tumor-initiating capabilities that underpin primary tumor growth, and CSCs endowed with dual tumor-initiating and metastatic competencies that fuel metastatic outgrowths. The finding that inhibition of p38-FOXC2 signaling impedes only metastasis, and not the primary tumor, suggests that the p38-FOXC2 signaling pathway could serve to distinguish tumor-initiating CSCs from metastasis-competent CSCs. In addition, it is well known that p38 is an important factor in MAPK signaling, which is involved in numerous cellular processes. Use of p38 inhibitors to intervene in the downstream signaling cascade of the MAPK pathway may interfere with many cellular activities in addition to the interruption of the p38–FOXC2–EMT axis. Although our data clearly provide evidence in support of this axis, it is also possible that other cellular signaling molecules, in addition to FOXC2, may function in different cellular contexts or tumor types.

Our findings that the phosphomimetic FOXC2(S367E) mutant is refractory to p38 inhibition and that the non-phosphorylatable FOXC2(S367A) mutant fails to elicit EMT underscore the importance of the evolutionarily conserved S367 residue for the biological functions of FOXC2. However, although FOXC2 is a transcription factor, it was unclear how activation of the p38-FOXC2 signaling axis might elicit suppression of E-cadherin and engage the EMT program. Our study identifies ZEB1—known to directly repress *E-cadherin*/*CDH1*, elicit EMT and confer CSC properties[35,36]—as a downstream target of FOXC2, critically dependent on its activation by p38. Moreover, both the p38 inhibitor SB203580 and p38 shRNA decrease FOXC2 protein levels, but not the mRNA, in a proteasome-dependent manner (Figure 1 and Supplementary Figure S1). However, how inhibition of phosphorylation by p38 targets FOXC2 for degradation is unclear. Amino acid sequence analysis of FOXC2 revealed a potential site for an E3 ubiquitin ligase, which may target FOXC2 for degradation by the proteasome, but this needs further investigation.

Independent studies have found elevated FOXC2 levels in metastatic[5,6] and residual therapy-resistant[7] breast tumors and implicated constitutive p38 signaling in the progression of metaplastic breast cancers,[37] the emergence of therapy resistance[38–40] and the tumor-promoting activities of carcinoma-associated fibroblasts.[41] Our data suggest a possible link between FOXC2 elevation and p38 activation in metastasis-prone

breast tumors. In conclusion, our study links p38-mediated phosphorylation of FOXC2 to the regulation of its downstream target ZEB1, EMT, stem cell traits and metastatic competence and attests to the potential utility of p38 inhibitors to attenuate FOXC2-dependent metastasis.

MATERIALS AND METHODS

Cell culture

Authenticated immortalized HMLE cells expressing empty vector (pWZL), Snail, Twist, Goosecoid or an activated form of TGFβ1, V12H-Ras-transformed HMLE (HMLER) and HMLER-FOXC2 cells were obtained from Dr Robert Weinberg (MIT) and maintained as previously described.[6,9] For 4-OHT treatment, HMLE-Snail-ER or HMLE-Twist-ER cells were exposed to 20 nM 4-OHT for the indicated number of days. MCF7, MDA-MB-231 and SUM159 human breast cancer cells[6] and the 4T1 mouse mammary carcinoma cells[13] were cultured as described. Human non-tumorigenic MCF10A cells were cultured as described[6] and treated with 2.5 ng/ml TGFβ1 for 3 days to elicit EMT. Cells were cultured for 24 h before addition of 20 μM SB203580 (Calbiochem, San Diego, CA, USA). All cell lines used for this study were recently confirmed negative for mycoplasma contamination.

Plasmids, shRNA and transduction

The expression vectors encoding HA-tagged p38 (HA-p38) and kinase-dead p38 (HA-p38-DN) have been described.[42] FOXC2 was PCR-amplified from pBabePuro-FOXC2 and subcloned into pcDNA3.1/myc-His vector. FOXC2-mutant constructs were generated by site-directed mutagenesis and subcloned into the retroviral vector MSCV-IRES-GFP. The primers used were: FOXC2(S367E) forward, 5′-CGAGCGGCCCCACGGAGCCCCTGAGCGC TCTCAACC-3′; reverse, 5′-GGTTGAGAGCGCTCAGGGGCTCCGTGGGGCCG CTCG-3′ and FOXC2(S367A) forward, 5′-CGAGCGGCCCCACGGCACCCCTG AGCGCTCTCAACC-3′; reverse, 5′-GGTTGAGAGCGCTCAGGGGTGCCGTGGGG CCGCTCG-3′.

To suppress p38 and FOXC2 expression, the shRNA-expressing lentivirus system was used (Open Biosystems, Huntsville, AL, USA). The shRNA sequences targeting p38 and FOXC2 were TTCACAGCTA GATTACTAG and CCTGAGCGAGCAGAATTACTA, respectively. shRNA targeting firefly luciferase (shControl) was used as a control. Lentiviral or retroviral transduction of target cells was performed as described previously.[43] Stable transductants were selected in 2 μg/ml puromycin.

Immunoblotting, immunofluorescence and antibodies

Immunoblotting[2] and immunofluorescence[3] were performed as previously described. Primary antibodies were as follows: β-actin (Sigma, St Louis, MO, USA; A3853), mouse anti-human FOXC2 and rat anti-mouse FOXC2 that also crossreacts with human FOXC2 (both developed by Dr Naoyuki Miura, Hamamatsu University School of Medicine, Hamamatsu, Japan), p-p38 (Cell Signaling, Danvers, MA, USA; 4511), p38 (Cell Signaling; 9211), E-cadherin (BD Biosciences, San Jose, CA, USA; 61081), fibronectin (BD Biosciences; 610077), vimentin (Novus Biologicals, Littleton, CO, USA; NB200-623), ZEB1 (Novus Biologicals; NBP1-05987), c-Myc (Santa Cruz Biotechnology, Dallas, TX, USA; sc-40), and HA (Covance, Princeton, NJ, USA; MMS-101P).

Co-immunoprecipitation

Cell lysates were incubated with antibodies overnight at 4 °C. Protein A/G-agarose beads (50 μl; Pierce, Waltham, MA, USA) were added for 12 h at 4 °C. The beads were washed with ice-cold radioimmunoprecipitation buffer (Sigma) containing protease and phosphatase inhibitors (Roche, Nutley, NJ, USA). Bound proteins were eluted by boiling in sample buffer, resolved by SDS–PAGE (sodium dodecyl sulfate–polyacrylamide gel electrophoresis) and analyzed by immunoblotting.

In vitro kinase assays

Glutathione-*S*-transferase-(GST)-tagged FOXC2 truncation mutants were subcloned into pGEX-6P-1 and expressed in *Escherichia coli*. Cell lysates were cleared by centrifugation and the GST-FOXC2 fusion proteins were absorbed on glutathione–sepharose-4B beads (Sigma) for 2 h at 4 °C. The beads were washed with lysis buffer and the GST-FOXC2 fusion proteins were eluted with reduced glutathione. The eluates (200 ng) were incubated with 100 ng of recombinant active p38α (Invitrogen, Grand Island, NY, USA; PV3304) in the presence of 60 mM $MgCl_2$, 60 μM ATP, 50 mM Tris-HCl (pH 7.5), 12 mM dithiothreitol, protease and phosphatase inhibitors (Roche) and 0.7 μCi of [γ-^{32}P]ATP, at room temperature for 30 min.

Quantitative reverse transcriptase–PCR

qRT-PCR was performed using SYBR Green (Applied Biosystems, Waltham, MA, USA) for mRNAs and Taqman (Applied Biosystems) for microRNAs as described previously.[6,44,45]

Chromatin immunoprecipitation

Chromatin immunoprecipitation was performed as described previously.[6]

Assays for EMT and stem cell properties

Quantification of invadopodia,[20] scratch/wound-healing assays,[45] fluorescence-activated cell sorting[3] and sphere-formation assays[3] were conducted as described previously.

Animal studies

NOD/SCID and BALB/c mice were purchased from the Jackson Laboratory (Bar Harbor, ME, USA). All mouse procedures were approved by the Animal Care and Use Committee of the University of Texas MD Anderson Cancer Center. To examine primary tumor formation and spontaneous metastasis, RFP/luciferase-labeled 4T1 cells (1×10^4 or 5×10^4) were injected into the inguinal mammary fat pad of 6-week-old female BALB/c mice. For experimental metastasis studies, 0.5×10^6 luciferase-labeled MDA-MB-231 cells were injected into 6-week-old female NOD/SCID mice via the tail vein. Thereafter, mice were randomized into groups, and vehicle or SB203580 (0.2 μmols in 100 μl per ~20 g mouse) was administered subcutaneously (once daily; 5 days/week). Mice were assessed weekly for tumor growth and metastasis via subcutaneous injection of D-Luciferin (150 mg/kg; Caliper LifeSciences, Hopkinton, MA, USA) and bioluminescent imaging (IVIS imaging system 200 series; Xenogen Corporation, PerkinElmer, Waltham, MA, USA). Investigators were blinded to the group allocation while assessing experimental outcomes. Primary tumor size was measured with a caliper as the product of two perpendicular diameters (mm^2). At the indicated time points, primary tumors and lungs were surgically excised, imaged and processed for histology.

Enumeration of CTCs

Mice were orthotopically injected with RFP/luciferase-labeled 4T1 cells. Starting week 3 post-injection, blood was collected, via cardiac puncture, in EDTA-coated tubes and treated with Ammonium-Chloride-Potassium lysing buffer (Invitrogen). Cells were cultured in RPMI-1640 medium containing 10% fetal bovine serum and penicillin/streptomycin. RFP-positive colonies were counted after 3 days.

Statistical analyses

Unless otherwise stated, all samples were assayed in triplicate. All *in vitro* experiments were repeated at least three independent times, and all animal experiments included at least five mice per group in each study. Unless otherwise indicated, data are represented as mean ± s.e.m., and significance was calculated using Student's unpaired two-tailed *t*-test.

CONFLICT OF INTEREST

SJW, NS, ANP, RS and SAM are inventors of a patent application based on the work described here. The remaining authors declare no conflict of interest.

ACKNOWLEDGEMENTS

We acknowledge Dr Mike Lewis, Dr Patricia Thompson and Dr Jody Vykoukal for helpful discussions. We particularly thank Dr Jonathan Kurie, Dr Robert Weinberg and Dr Mien-Chie Hung for critically reading the manuscript. This research was supported by grants from the National Institute of Health (5RO1CA155243) and the Cancer Prevention and Research Institute of Texas (RP-130485). SAM is an American Cancer Society M Patricia Alexander Research Scholar (121958-RSG-12-102-01-DDC). SJW received a Susan G Komen Breast Cancer Foundation Postdoctoral Fellowship. Flow cytometry, animal imaging and histopathology were in part funded by the Cancer Center Support Grant from the National Cancer Institute (5P30CA016672).

REFERENCES

1 Gupta GP, Massague J. Cancer metastasis: building a framework. *Cell* 2006; **127**: 679–695.
2 Tsai JH, Yang J. Epithelial-mesenchymal plasticity in carcinoma metastasis. *Genes Dev* 2013; **27**: 2192–2206.
3 Mani SA, Guo W, Liao MJ, Eaton EN, Ayyanan A, Zhou AY *et al.* The epithelial-mesenchymal transition generates cells with properties of stem cells. *Cell* 2008; **133**: 704–715.
4 Morel AP, Lievre M, Thomas C, Hinkal G, Ansieau S, Puisieux A. Generation of breast cancer stem cells through epithelial-mesenchymal transition. *PLoS One* 2008; **3**: e2888.
5 Mani SA, Yang J, Brooks M, Schwaninger G, Zhou A, Miura N *et al.* Mesenchyme Forkhead 1 (FOXC2) plays a key role in metastasis and is associated with aggressive basal-like breast cancers. *Proc Natl Acad Sci USA* 2007; **104**: 10069–10074.
6 Hollier BG, Tinnirello AA, Werden SJ, Evans KW, Taube JH, Sarkar TR *et al.* FOXC2 expression links epithelial-mesenchymal transition and stem cell properties in breast cancer. *Cancer Res* 2013; **73**: 1981–1992.
7 Creighton CJ, Li X, Landis M, Dixon JM, Neumeister VM, Sjolund A *et al.* Residual breast cancers after conventional therapy display mesenchymal as well as tumor-initiating features. *Proc Natl Acad Sci USA* 2009; **106**: 13820–13825.
8 Obenauer JC, Cantley LC, Yaffe MB. Scansite 2.0: proteome-wide prediction of cell signaling interactions using short sequence motifs. *Nucleic Acids Res* 2003; **31**: 3635–3641.
9 Elenbaas B, Spirio L, Koerner F, Fleming MD, Zimonjic DB, Donaher JL *et al.* Human breast cancer cells generated by oncogenic transformation of primary mammary epithelial cells. *Genes Dev* 2001; **15**: 50–65.
10 Kumar S, Jiang MS, Adams JL, Lee JC. Pyridinylimidazole compound SB 203580 inhibits the activity but not the activation of p38 mitogen-activated protein kinase. *Biochem Biophys Res Commun* 1999; **263**: 825–831.
11 Yan C, Grimm WA, Garner WL, Qin L, Travis T, Tan N *et al.* Epithelial to mesenchymal transition in human skin wound healing is induced by tumor necrosis factor-alpha through bone morphogenic protein-2. *Am J Pathol* 2010; **176**: 2247–2258.
12 Aomatsu K, Arao T, Abe K, Kodama A, Sugioka K, Matsumoto K *et al.* Slug is upregulated during wound healing and regulates cellular phenotypes in corneal epithelial cells. *Invest Ophthalmol Vis Sci* 2012; **53**: 751–756.
13 Aslakson CJ, Miller FR. Selective events in the metastatic process defined by analysis of the sequential dissemination of subpopulations of a mouse mammary tumor. *Cancer Res* 1992; **52**: 1399–1405.
14 Pulaski BA, Ostrand-Rosenberg S. Mouse 4T1 breast tumor model. In: Coligan JE, Kruisbeek AM, Margulies DH, Shevach EM, Strober W (eds). *Current Protocols in Immunology*, Supplement 39, Chapter 20. John Wiley and Sons, Inc., 2001, pp 20.2.1–20.2.16.
15 Yoshizuka N, Chen RM, Xu Z, Liao R, Hong L, Hu WY *et al.* A novel function of p38-regulated/activated kinase in endothelial cell migration and tumor angiogenesis. *Mol Cell Biol* 2012; **32**: 606–618.
16 Kume T. The role of FoxC2 transcription factor in tumor angiogenesis. *J Oncol* 2012; **2012**: 204593.
17 Pantel K, Cote RJ, Fodstad O. Detection and clinical importance of micrometastatic disease. *J Natl Cancer Inst* 1999; **91**: 1113–1124.
18 Fehm T, Muller V, Alix-Panabieres C, Pantel K. Micrometastatic spread in breast cancer: detection, molecular characterization and clinical relevance. *Breast Cancer Res* 2008; **10**(Suppl 1): S1.
19 Valastyan S, Weinberg RA. Tumor metastasis: molecular insights and evolving paradigms. *Cell* 2011; **147**: 275–292.
20 Eckert MA, Lwin TM, Chang AT, Kim J, Danis E, Ohno-Machado L *et al.* Twist1-induced invadopodia formation promotes tumor metastasis. *Cancer Cell* 2011; **19**: 372–386.
21 Al-Hajj M, Wicha MS, Benito-Hernandez A, Morrison SJ, Clarke MF. Prospective identification of tumorigenic breast cancer cells. *Proc Natl Acad Sci USA* 2003; **100**: 3983–3988.
22 Burk U, Schubert J, Wellner U, Schmalhofer O, Vincan E, Spaderna S *et al.* A reciprocal repression between ZEB1 and members of the miR-200 family promotes EMT and invasion in cancer cells. *EMBO Rep* 2008; **9**: 582–589.
23 Gregory PA, Bert AG, Paterson EL, Barry SC, Tsykin A, Farshid G *et al.* The miR-200 family and miR-205 regulate epithelial to mesenchymal transition by targeting ZEB1 and SIP1. *Nat Cell Biol* 2008; **10**: 593–601.
24 Darnell JE Jr. Transcription factors as targets for cancer therapy. *Nat Rev Cancer* 2002; **2**: 740–749.
25 Huang S, New L, Pan Z, Han J, Nemerow GR. Urokinase plasminogen activator/urokinase-specific surface receptor expression and matrix invasion by breast cancer cells requires constitutive p38alpha mitogen-activated protein kinase activity. *J Biol Chem* 2000; **275**: 12266–12272.
26 Emerling BM, Platanias LC, Black E, Nebreda AR, Davis RJ, Chandel NS. Mitochondrial reactive oxygen species activation of p38 mitogen-activated protein kinase is required for hypoxia signaling. *Mol Cell Biol* 2005; **25**: 4853–4862.
27 del Barco Barrantes I, Nebreda AR. Roles of p38 MAPKs in invasion and metastasis. *Biochem Soc Trans* 2012; **40**: 79–84.
28 Vecchi M, Confalonieri S, Nuciforo P, Vigano MA, Capra M, Bianchi M *et al.* Breast cancer metastases are molecularly distinct from their primary tumors. *Oncogene* 2008; **27**: 2148–2158.
29 Steeg PS, Theodorescu D. Metastasis: a therapeutic target for cancer. *Nat Clin Pract Oncol* 2008; **5**: 206–219.
30 Blanco MA, Kang Y. Signaling pathways in breast cancer metastasis - novel insights from functional genomics. *Breast Cancer Res* 2011; **13**: 206.
31 Malinowsky K, Wolff C, Berg D, Schuster T, Walch A, Bronger H *et al.* uPA and PAI-1-related signaling pathways differ between primary breast cancers and lymph node metastases. *Transl Oncol* 2012; **5**: 98–104.
32 Brabletz T, Jung A, Spaderna S, Hlubek F, Kirchner T. Opinion: migrating cancer stem cells - an integrated concept of malignant tumour progression. *Nat Rev Cancer* 2005; **5**: 744–749.
33 Hermann PC, Huber SL, Herrler T, Aicher A, Ellwart JW, Guba M *et al.* Distinct populations of cancer stem cells determine tumor growth and metastatic activity in human pancreatic cancer. *Cell Stem Cell* 2007; **1**: 313–323.
34 Liu S, Cong Y, Wang D, Sun Y, Deng L, Liu Y *et al.* Breast cancer stem cells transition between epithelial and mesenchymal states reflective of their normal counterparts. *Stem Cell Rep* 2014; **2**: 78–91.
35 Eger A, Aigner K, Sonderegger S, Dampier B, Oehler S, Schreiber M *et al.* DeltaEF1 is a transcriptional repressor of E-cadherin and regulates epithelial plasticity in breast cancer cells. *Oncogene* 2005; **24**: 2375–2385.
36 Wellner U, Schubert J, Burk UC, Schmalhofer O, Zhu F, Sonntag A *et al.* The EMT-activator ZEB1 promotes tumorigenicity by repressing stemness-inhibiting microRNAs. *Nat Cell Biol* 2009; **11**: 1487–1495.
37 Hennessy BT, Gonzalez-Angulo AM, Stemke-Hale K, Gilcrease MZ, Krishnamurthy S, Lee JS *et al.* Characterization of a naturally occurring breast cancer subset enriched in epithelial-to-mesenchymal transition and stem cell characteristics. *Cancer Res* 2009; **69**: 4116–4124.
38 Gutierrez MC, Detre S, Johnston S, Mohsin SK, Shou J, Allred DC *et al.* Molecular changes in tamoxifen-resistant breast cancer: relationship between estrogen receptor, HER-2, and p38 mitogen-activated protein kinase. *J Clin Oncol* 2005; **23**: 2469–2476.
39 Donnelly SM, Paplomata E, Peake BM, Sanabria E, Chen Z, Nahta R. P38 MAPK contributes to resistance and invasiveness of HER2-overexpressing breast cancer. *Curr Med Chem* 2014; **21**: 501–510.
40 Kopper F, Binkowski AM, Bierwirth C, Dobbelstein M. The MAPK-activated protein kinase 2 mediates gemcitabine sensitivity in pancreatic cancer cells. *Cell Cycle* 2014; **13**: 884–889.
41 Alspach E, Flanagan KC, Luo X, Ruhland MK, Huang H, Pazolli E *et al.* p38MAPK plays a crucial role in stromal-mediated tumorigenesis. *Cancer Discov* 2014; **4**: 716–729.
42 Kawano H, Kim S, Ohta K, Nakao T, Miyazaki H, Nakatani T *et al.* Differential contribution of three mitogen-activated protein kinases to PDGF-BB-induced mesangial cell proliferation and gene expression. *J Am Soc Nephrol* 2003; **14**: 584–592.
43 Stewart SA, Dykxhoorn DM, Palliser D, Mizuno H, Yu EY, An DS *et al.* Lentivirus-delivered stable gene silencing by RNAi in primary cells. *RNA* 2003; **9**: 493–501.
44 Taube JH, Malouf GG, Lu E, Sphyris N, Vijay V, Ramachandran PP *et al.* Epigenetic silencing of microRNA-203 is required for EMT and cancer stem cell properties. *Sci Rep* 2013; **3**: 2687.
45 Sarkar TR, Battula VL, Werden SJ, Vijay GV, Ramirez-Pena EQ, Taube JH *et al.* GD3 synthase regulates epithelial-mesenchymal transition and metastasis in breast cancer. *Oncogene* 2015; **34**: 2958–2967.

Supplementary Information accompanies this paper on the Oncogene website (http://www.nature.com/onc)